ACS APPLIED MATERIALS & INTERFACES

Research Article

www.acsami.org

Highly Transparent Wafer-Scale Synthesis of Crystalline WS_2 Nanoparticle Thin Film for Photodetector and Humidity-Sensing Applications

Amit S. Pawbake,[†,‡] Ravindra G. Waykar,[‡] Dattatray J. Late,[*,†] and Sandesh R. Jadkar[*,‡]

[†]Physical and Material Chemistry Division, CSIR – National Chemical Laboratory, Pune, 411008 Maharashtra, India

[‡]School of Energy Studies, Department of Physics, Savitribai Phule Pune University, Pune, 411007 Maharashtra, India

Supporting Information

ABSTRACT: In the present investigation, we report a one-step synthesis method of wafer-scale highly crystalline tungsten disulfide (WS_2) nanoparticle thin film by using a modified hot wire chemical vapor deposition (HW-CVD) technique. The average size of WS_2 nanoparticle is found to be 25−40 nm over an entire 4 in. wafer of quartz substrate. The low-angle XRD data of WS_2 nanoparticle shows the highly crystalline nature of sample along with orientation (002) direction. Furthermore, Raman spectroscopy shows two prominent phonon vibration modes of E^1_{2g} and A_{1g} at ∼356 and ∼420 cm^{-1}, respectively, indicating high purity of material. The TEM analysis shows good crystalline quality of sample. The synthesized WS_2 nanoparticle thin film based device shows good response to humidity and good photosensitivity along with good long-term stability of the device. It was found that the resistance of the films decreases with increasing relative humidity (RH). The maximum humidity sensitivity of 469% along with response time of ∼12 s and recovery time of ∼13 s were observed for the WS_2 thin film humidity sensor device. In the case of photodetection, the response time of ∼51 s and recovery time of ∼88 s were observed with sensitivity ∼137% under white light illumination. Our results open up several avenues to grow other transition metal dichalcogenide nanoparticle thin film for large-area nanoelectronics as well as industrial applications.

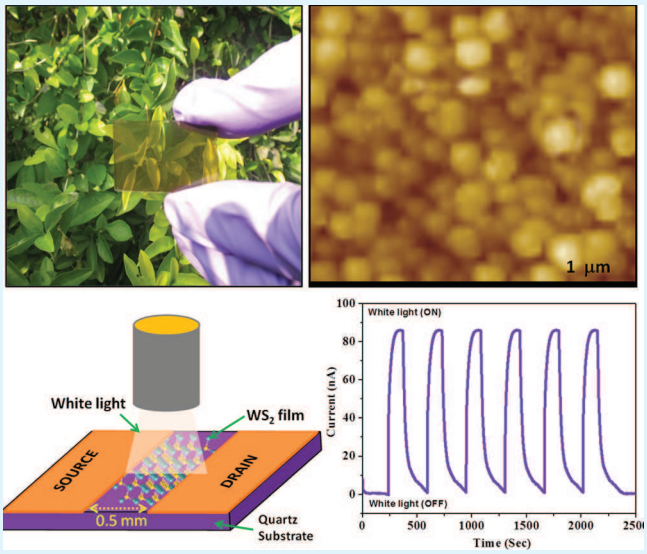

KEYWORDS: *tungsten disulfide, nanoparticle, thin film, chemical vapor deposition, humidity sensor, photosensor*

INTRODUCTION

Graphene was thought not to exist in a free state until 2004, when Novoselov and co-workers isolated a single-atom-thick layer of carbon.[1] Since then, interest in graphene has grown continuously because of its extraordinary electrical, optical, magnetic, and mechanical properties. Graphene has attracted more attention in nanoelectronics and optoelectronics devices because of its huge mobility ∼200 000 $cm^2/(V\ s)$ and ultrafast speed in radio frequency communication devices. The only disadvantage of graphene is the low I_{on}/I_{off} ratio; as a result, it is difficult to switch off the electronic devices because of the lack of band gap. Graphene analogues of transition metal dichalcogenides (TMDCs) semiconducting layered materials have attracted much more attention because of tunable, wide, and direct band gap with good mobility of ∼500 $cm^2/(V\ s)$ and a good I_{on}/I_{off} ratio of $\sim 10^8$.[2−13] Recently, Kalantar-zadeh et al. reported that TMDCs have potential to be used in biological systems because of their tunable optoelectrical properties, highly stability, large surface area, and low levels of toxicity.[14]

Bulk WS_2 is an indirect band gap (1.4 eV) semiconductor; when thin to monolayer, the band gap becomes wide and direct (2.1 eV). Each single layer of WS_2 comprises a trilayer of atoms composed of a tungsten layer sandwiched between two sulfur layers in a trigonal prismatic coordination so that structure resembles S−W−S,[15] and the 2H−WS_2 polytype crystalline structure has the hexagonal space group $P6_3/mmc$ with lattice parameters of a = 3.1532 Å and c = 12.323 Å.[15,16] Because of its excellent optical, electrical, and mechanical properties, WS_2 nanosheets has been widely used for various applications including field emission,[17] lubrication coatings,[18] field-effect transistors,[19] sensors,[20] antibacterial activities,[21] and water

Received: November 23, 2015
Accepted: January 14, 2016
Published: January 14, 2016

DOI: 10.1021/acsami.5b11325
ACS Appl. Mater. Interfaces 2016, 8, 3359−3365

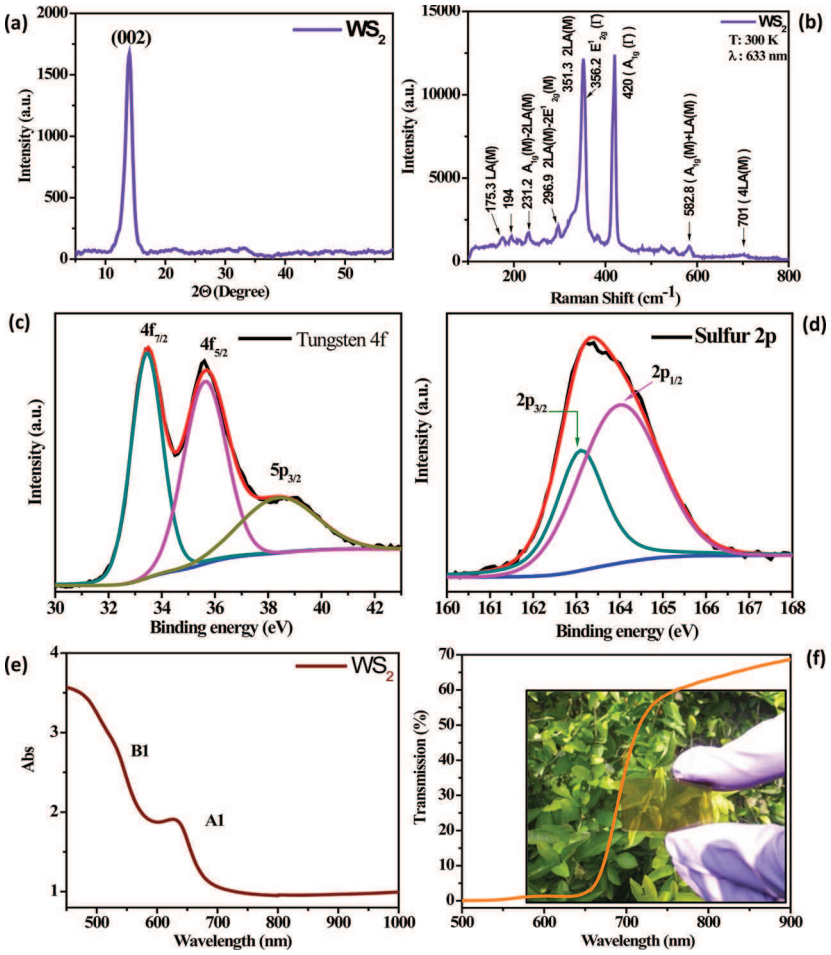

Figure 1. HW-CVD-grown WS_2 nanoparticle thin film characteristics. (a) XRD pattern, (b) Raman spectrum, (c) deconvoluted XPS scan for tungsten 4f, (d) deconvoluted XPS scan for sulfur 2p, (e) UV−visible absorption spectra, and (f) transmittance spectra. Inset of f shows the optical photograph of typical WS_2 nanoparticle thin film grown on quartz substrate.

splitting,[22] amon others. To date, atomically thin few-layer WS_2 has been successfully grown by various methods including mechanical exfoliation,[23] annealing $(NH_4)_2WS_4$ thin films,[24] wet chemical approaches,[25] physical vapor deposition,[26] and sulfurization of tungsten foil at high temperature.[27]

HW-CVD and CVD are predicted to be a capable method to produce large-area, uniform TMDCs sheets and nanostructures for a wide range of device applications from the perspective of the repeatability and controllability. A two-step process has been reported earlier to grow centimeter-size[28] as well as wafer-scale nonuniform synthesis of WS_2 nanosheets using predeposition and sulfurization of WO_3 film on SiO_2.[29] It is important to note that single-crystalline and large-area WS_2 single-layer nanosheets with the size of hundreds of micrometers have been synthesized on SiO_2/Si substrates in CVD system using WO_3 powder.[30] Kalantar-zadeh et al. also reported a three-step process for atomically thin WO_3.[31]

In view of the growth on SiO_2 substrate that acts as preferred nucleation growth site for the TMDCs nanosheets behind the terrace of the substrate nonuniformity, another disadvantage that is the surface remains mostly hydrophilic oxide. The quartz substrate seems to be more promising and suitable to grow the large-area uniform and highly crystalline TMDCs because of the matching of lattice symmetry.[28,29,32] Zhang et al.[33] reported the synthesis of highly crystalline WS_2 nanosheets with size up to 50 × 50 μm^2 on *c*-sapphire substrate using CVD. The uses of the HW-CVD system to prepare controllable WS_2 nanoparticle film in one-step growth conditions are therefore more advantageous. More importantly, the low adhesion of WS_2 film can also be used to transfer the WS_2 film on to the desired substrate for wide and useful applications. Considering this fact and the cost of the SiO_2 as well as sapphire substrates, it is enormously significant to develop a method to recycle a substrate to lower the cost of growing highly crystalline TMDCs for large-scale industrial applications.

We present uniform and large-area 4 in. wafer-scale synthesis of WS_2 nanoparticle thin film using HW-CVD method and its application toward humidity and photosensing.

RESULTS AND DISCUSSION

We have successfully synthesized highly crystalline WS_2 nanoparticle thin film with thickness of 25−40 nm. Highly crystalline hexagonal structure of WS_2 thin film was confirmed using X-ray Ddiffraction (XRD), as shown in Figure 1a. From the XRD data, it is clear that the orientation of WS_2 nanoparticle film is along (002) plane. Typical room-temperature Raman spectra for WS_2 nanoparticle film were recorded using a 632 nm laser source as shown in Figure 1b. Raman spectra show two prominent phonon vibration modes, E^1_{2g} and A_{1g}, at ∼356 and ∼420 cm^{-1}, respectively, along with other lower intensity peaks seen in the spectra. Figure 1c shows typical deconvoluted XPS scan for tungsten (4f) of WS_2 thin

DOI: 10.1021/acsami.5b11325
ACS Appl. Mater. Interfaces 2016, 8, 3359−3365

film; the W (4f) peak in the range of 31−42 eV was observed, which is further deconvoluted into the three component bands near 33.1, 35.8, and 38.7 eV assigned to W $4f_{7/2}$, W $4f_{5/2}$, and W $5p_{3/2}$, respectively. Figure 1d shows typical deconvoluted XPS scan for sulfur (2p) of WS_2 thin film; the S (2p) peak in the range of 161−167 eV was observed, which is further deconvoluted into the two component bands near 162.9 and 164.1 eV assigned to S $2p_{1/2}$ and S $2p_{3/2}$. Figure 1e shows absorption spectra for WS_2; two typical characteristic absorption peaks of WS_2 were clearly observed at the region of 500−700 nm, which corresponds to the A1 and B1 direct exciton transitions of the WS_2 originating from the energy split of valence band and spin−orbital coupling.[34] Figure 1f shows the transmittance spectra recorded between 200 and 900 nm. The inset of Figure 1f shows the optical photograph of typical WS_2 nanoparticle thin film grown on quartz substrate.

Figure 2a shows the FESEM image of the WS_2 nanoparticle thin film sample, which shows a small spherical nanoparticle

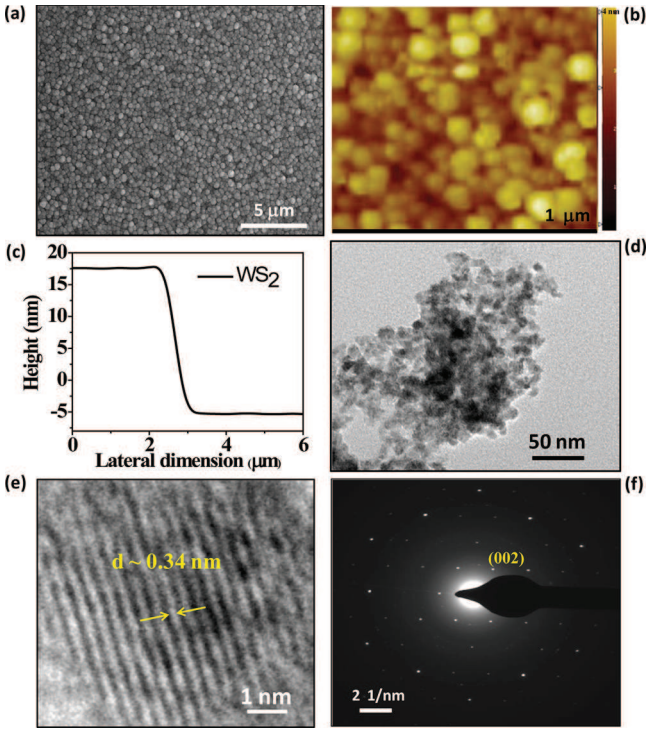

Figure 2. HW-CVD-deposited WS_2 nanoparticle thin film. (a) Typical FESEM image, (b) AFM image, (c) AFM height profile, (d) low-magnification TEM image, (e) high-resolution TEM image, and (f) typical SAED pattern.

morphology. Figure 2b shows the typical AFM image of WS_2 nanoparticle thin film. Further AFM depicts the WS_2 film as consisting of a uniform nanoparticle with average size ~20 nm. Figure 2c shows the typical AFM height profile of WS_2 thin film and shows the average thickness of film as 25−40 nm. Figure 2d shows low-magnification TEM image and the ~20 nm size nanoparticle of WS_2. Figure 2e shows the high-resolution TEM (HRTEM) image with d spacing ~0.34 nm. Figure 2f shows the corresponding selected area electron diffraction pattern (SAED) with indexing for the WS_2 nanoparticle, which shows highly crystalline nature of the sample. From various optimized experiments, we observed that the filament temperature is key parameter for getting morphology of WS_2 thin film.

Figure 3a shows the schematic diagram of the device fabricated for humidity and photosensing experiments. In a photodetector, photon absorption generates extra free carriers, reducing the electrical resistance of the semiconductor because of the photo-generated free electrons and holes that drift in opposite directions toward the metal leads, resulting in a net increase in the current. Photocurrent strongly depends on electron−hole separation and thermal mechanisms.[35] Figure 3b shows a typical current versus voltage (I−V) curve in the range of −5 to +5 V for WS_2 nanoparticle thin film device under dark and illumination light conditions. From the I−V curve, it is seen that the current increases because of illumination which confirms the semiconducting behavior of the as-deposited WS_2 nanoparticle thin film. Figure 3c shows current versus time (I−t) plot for WS_2-based photosensor device at constant 0.2 V bias voltages for 2 min illumination and 3 min dark conditions. Figure 3d shows a single-cycle I−t curve for measuring response and recovery time, which are ~51 s and ~88 s, respectively. Response time is defined as the time required for a photodetector to reach 90% of the maximum photocurrent value from its dark current value. Similarly, decay time is defined as the time required for photodetector reaching 10% of maximum photocurrent response. The photosensitivity of the WS_2 nanoparticle thin film based device was found to be 137%, using the relation of photosensitivity[36]

$$\text{Photosensitivity (\%)} = \frac{I_{\text{photo}} - I_{\text{dark}}}{I_{\text{dark}}}$$

Photosensitivity (%) is defined as the ratio between the difference in photo current (I_{photo}) and dark current (I_{dark}) values to the dark current. The comparisons for TMDCs photosensor are listed in Table 1.

The humidity-sensing properties were investigated by fabricating the two probe device and then introducing the device to different relative humidity (RH) conditions, which were attained by saturated salt solutions at room temperature. Figure 4a shows the I−V characteristics of WS_2 sensor at different RH levels. From the I−V curve, it is clear that the current increases with the increase in relative humidity implying that the H_2O molecules present in the saturated salts act as electron donor and results in n-type doping. The water molecules present in the saturated salts adsorbed on the surface of WS_2 nanoparticle thin film shift the Fermi level closer to the conduction band edge. Furthermore, the humidity sensing is based on the mechanism of adsorption of water molecules on the surface of material and proton conduction; the proton acts as an effective carrier for the electrical conductivity.[37] Figure 4b shows response and recovery time for WS_2-based sensors in a changing humidity environment (from a minimum of 11.3% to a maximum of 97.3% in the time interval of 30 s) at 0.5 V bias voltages. The calculated response time of ~12 s and recovery time of ~13 s were observed for the WS_2 nanoparticle thin film based sensor, which is shown in Figure 4 c. The fast recovery time may be due to the fast desorption process of H_2O molecules from the WS_2 nanoparticle, and the slow response is due to hydrophilic surface of the WS_2 nanoparticle resulting in slow adsorption of H_2O molecules on the surface of nanoparticle.

Figure 4d shows the sensitivity versus relative humidity plot, which shows an increase in sensitivity with increase in relative humidity. The sensitivity is defined as[36]

DOI: 10.1021/acsami.5b11325
ACS Appl. Mater. Interfaces 2016, 8, 3359−3365

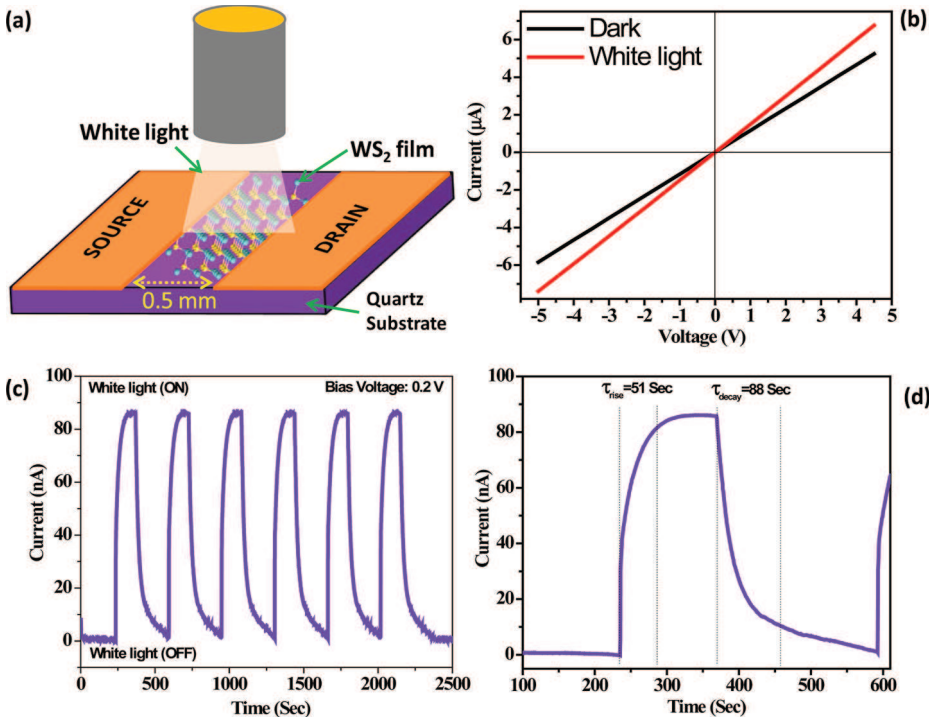

Figure 3. WS_2 nanoparticle thin film based photosensor device characteristics. (a) Schematic of sensor device, (b) typical current−voltage (I−V) characteristics for dark and under white light illumination, (c) current vs time plot for dark and under white light illumination conditions, and (d) current vs time plot for response and recovery time measurement.

Table 1. Comparison of 2D-Layered Materials Based Photosensors Reported in the Literature

TMDCs	synthesis method	response time	recovery time	ref
MoS_2	mechanically exfoliated	1.8 ms	2 ms	38
		50 ms	50 ms	39
		20 s	10.97 s	40
	CVD	1.79 s	1.23 s	41
$MoSe_2$	CVD	60 ms	60 ms	44
	PLD	4.1 s	4.4 s	42
WS_2	CVD	60 ms	190 ms	43
	HW-CVD	51 ± 5 s	88 ± 6 s	present work

$$\text{Sensitivity}\ (\%) = \frac{R_{11\%} - R_{97\%}}{R_{97\%}} \times 100$$

where $R_{11.3\%}$ and $R_{97\%}$ are the resistances of the device at lower humidity and after the change in humidity, respectively. The comparisons for TMDCs photosensor are listed in Table 2.

CONCLUSIONS

We have successfully synthesized 4 in. industrial-scale highly crystalline WS_2 nanoparticle thin film by HW-CVD method. Furthermore, XRD and TEM analysis reveal the highly crystalline nature of WS_2 nanoparticle thin film, whereas AFM confirms the spherical size nanoparticles with average thickness of 25−40 nm. The humidity-sensing behaviors were investigated in the range of 11−97% relative humidity at room temperature. The maximum sensitivity of 469%, response time of ∼12 s, and recovery time of ∼13 s were observed for the WS_2 nanoparticle thin film based humidity sensor. In the case of photodetection, the response time is ∼51 s, and recovery time is ∼88 s, observed under white light illumination with sensitivity ≈ 137%. Our results indicate the potential of HW-CVD method to synthesize WS_2 and other TMDCs nanoparticle thin films in one step on an industrial scale for a wide range of applications including nano sensors, nanoelectronics, and energy-harvesting devices.

EXPERIMENTAL METHODS

Synthesis of WS_2 Thin Film. For WS_2 thin film, we used tungsten wire (0.5 mm diameter with 99.99% purity) and H_2S (99.99% purity) gas precursor. The typical reaction of WS_2 nanoparticle thin film synthesis is given below.

$$W_{(Solid)} + 2H_2S_{(gas)} \xrightarrow{\Delta} WS_{2(Solid)} + 2H_{2(gas)}$$

Because of high filament temperature and continuous bombardment of H_2S gas, tungsten itself can be incorporated in the thin film by forming WS_2 radicals. Before reaching the substrate, the radical and gas-phase reaction takes place. During deposition of WS_2 thin film, the temperature of the filament was maintained at 2000 °C, and the quartz substrate were kept at 800 °C.

Raman Spectroscopy. The WS_2 nanoparticle thin film was characterized with Renishaw microscope with laser wavelength of 632 nm in the back-scattering geometry. The detector used was a CCD synapse with thermoelectric cooling to −70 °C. A 50× objective was used to focus the laser beam and to collect the Raman signal. The laser power on the sample was ∼2 mW so as to avoid the possible heating effect by the laser on the samples. The peak positions, intensity, and line widths were extracted by fitting the experimental data with Lorentzian functions.

Transmission Electron Microscope. Transmission electron microscopic images and SAED pattern were recorded using a transmission electron microscope (TECNAI G^2-20-TWIN, FEI, The Netherlands) operating at 200 keV.

X-ray Diffraction. The XRD pattern of WS_2 thin film was recorded using X-ray diffractometer (Bruker D8 Advance, Germany) using the Cu Kα line (λ = 1.54056 Å).

DOI: 10.1021/acsami.5b11325
ACS Appl. Mater. Interfaces 2016, 8, 3359−3365

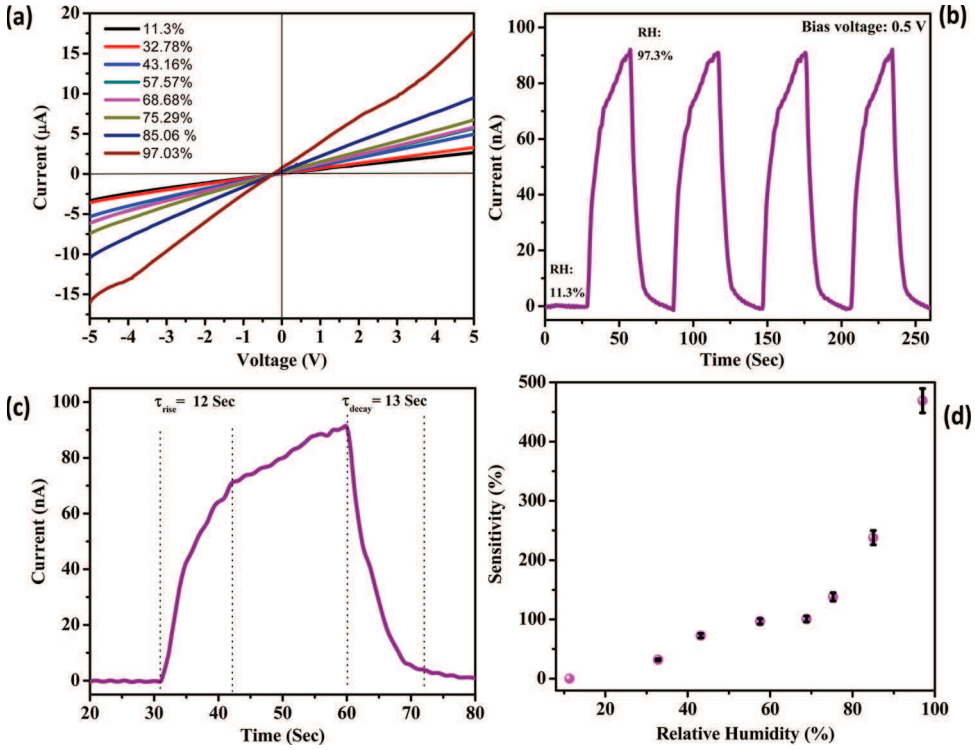

Figure 4. WS_2 nanoparticle thin film based humidity sensor device characteristics. (a) Typical current−voltage (I−V) characteristics for various relative humidity. (b) Typical response to 11.3 and 97.3% RH. (c) Current vs time plot for response and recovery time measurement and (d) typical plot of sensitivity vs relative humidity.

Table 2. Comparison of 2D-Layered Materials Based Humidity Sensor Reported in the Literature

TMDCs	synthesis method	response time (s)	recovery time (s)	ref
MoS_2	liquid exfoliation	9	17	45
VS_2	liquid exfoliation	30−40	25−50	46
WS_2	HW-CVD	12 ± 5	13 ± 5	present work

UV−Visible Spectroscopy. Transmittance and absorption spectra of the films deposited on Corning glass were measured using a JASCO, V-670 UV−visible spectrophotometer in the range of 200−1000 nm.

Field-Emission Scanning Electron Microscopy. The morphological study of the samples was carried out using a scanning electron microscope (FEI Nova NANOSEM 450)

X-ray Photoelectron Spectroscopy. For XPS, we used a VG Microtech apparatus (England, model name Multi-Lab, ESCA-3000, Sr. No. 8546/1, Multi-Lab). All experiments were carried out under ultrahigh vacuum (UHV).

Atomic Force Microscopy. Surface morphology and height profile were measured using Bruker's multicode 8 instrument using tapping mode.

Sensor Device Fabrication. The humidity sensor as well as photodetector devices were fabricated on a quartz substrate with Ag film as a source−drain electrode (separation = 0.5 mm), deposited using an electrode mask under vacuum evaporation technique.

Humidity Sensing. All the electrical measurements were carried out using Keithley 2612A system source meter that was attached to a computer through a GPIB 488A interface. The response of the device as a function of RH was performed by introducing the device to different RH levels. The relative humidity levels were obtained by keeping the saturated salts of LiCl, $MgCl_2$, K_2CO_3, NaBr, KI, NaCl, KCl, and K_2SO_4 in a closed vessel.

Photo Sensing. All the electrical measurements were carried out using a Keithley 2612A system source meter that was attached to a computer through a GPIB 488A interface. For white light illumination, a PEC-L01 Portable Solar Simulator was used for photodetection, which provided a wide-range spectrum from ultraviolet to near-IR.

■ ASSOCIATED CONTENT

Supporting Information

The Supporting Information is available free of charge on the ACS Publications website at DOI: 10.1021/acsami.5b11325.

Details of HW-CVD synthesis method. (PDF)

■ AUTHOR INFORMATION

Corresponding Authors

*E-mail: dj.late@ncl.res.in/datta099@gmail.com.
*E-mail: sandesh@physics.unipune.ac.in.

Notes

The authors declare no competing financial interest.

■ ACKNOWLEDGMENTS

This work was financially supported by DST and MNRE, Government of India and CNQS, Savitribai Phule Pune University, Pune 411 007. S.R.J. is grateful to University Grants Commission, New Delhi, for the financial support under UPE program. The research work was supported by Department of Science and Technology (Government of India) under Ramanujan Fellowship (Grant No. SR/S2/RJN-130/2012), NCL-MLP project grant 028626, DST-SERB Fast-track Young scientist project Grant No. SB/FT/CS-116/2013, Broad of Research in Nuclear Sciences (BRNS Grant No. 34/14/20/2015 (Government of India), and partial support by INUP IITB project sponsored by DeitY, MCIT, Government of India.

DOI: 10.1021/acsami.5b11325
ACS Appl. Mater. Interfaces 2016, 8, 3359−3365

REFERENCES

(1) Novoselov, K. S.; Jiang, D.; Schedin, F.; Booth, T. J.; Khotkevich, V. V.; Morozov, S. V.; Geim, A. K. Two-dimensional Atomic Crystals. *Proc. Natl. Acad. Sci. U. S. A.* **2005**, *102*, 10451−10453.

(2) Tenne, R.; Margulis, L.; Genut, M.; Hodes, G. Polyhedral and Cylindrical Structures of Tungsten Disulphide. *Nature* **1992**, *360*, 444−446.

(3) Margulis, L.; Salitra, G.; Tenne, R.; Talianker, M. Nested. Fullerene-like Structures. *Nature* **1993**, *365*, 113−114.

(4) Feldman, Y.; Wasserman, E.; Srolovitz, J.; Tenne, R. High-rate Gas-phase Growth of MoS_2 Nested Inorganic Fullerenes and Nanotubes. *Science* **1995**, *267*, 222−225.

(5) Thripuranthaka M; Late, D. J. Temperature Dependent Phonon Shifts in Single-layer WS_2. *ACS Appl. Mater. Interfaces* **2014**, *6*, 1158−1163.

(6) Late, D. J.; Shirodkar, S. N.; Waghmare, U. V.; Dravid, V. P.; Rao, C.N. R. Thermal Expansion, Anharmonicity and Temperature-Dependent Raman Spectra of Single-and Few-Layer $MoSe_2$ and WSe_2. *ChemPhysChem* **2014**, *15*, 1592−1598.

(7) Late, D. J. Temperature Dependent Phonon Shifts in Few-Layer Black Phosphorus. *ACS Appl. Mater. Interfaces* **2015**, *7*, 5857−5862.

(8) Castellanos-Gomez, A.; Poot, M.; Steele, G. A.; van der Zant, H. S. J.; Agraït, N.; Rubio-Bollinger, G. Elastic Properties of Freely Suspended MoS_2 Nanosheets. *Adv. Mater.* **2012**, *24*, 772−775.

(9) Late, D. J.; Liu, B.; Luo, J.; Yan, A.; Matte, H. S. S.; Grayson, M.; Rao, C. N. R.; Dravid, V. P. GaS and GaSe Ultrathin Layer Transistors. *Adv. Mater.* **2012**, *24*, 3549−3554.

(10) Pawbake, A. S.; Pawar, M. S.; Jadkar, S. R.; Late, D. J. Large Area Chemical Vapor Deposition of Monolayer Transition Metal Dichalcogenides and their Temperature Dependent Raman Spectroscopy Studies. *Nanoscale* **2016**, DOI: 10.1039/C5NR07401K.

(11) Pawbake, A. S.; Island, J. O.; Flores, E.; Ares, J. R.; Sanchez, C.; Ferrer, I. J.; Jadkar, S. R.; vander Zant, H. S.; Castellanos-Gomez, A.; Late, D. J. Temperature Dependent Raman Spectroscopy of Titanium Trisulfide (TiS_3) Nanoribbons and Nanosheets. *ACS Appl. Mater. Interfaces* **2015**, *7*, 24185−24190.

(12) Late, D. J.; Huang, Y.-K.; Liu, B.; Acharya, J.; Shirodkar, S. N.; Luo, J.; Yan, A.; Charles, D.; Waghmare, U. V.; Dravid, V. P.; Rao, C. N. R. Sensing Behavior of Atomically Thin-Layered MoS_2 Transistors. *ACS Nano* **2013**, *7*, 4879−4891.

(13) Buscema, M.; Groenendijk, D. J.; Blanter, S. I.; Steele, G. A.; van der Zant, H. S. J.; Castellanos-Gomez, A. Fast and Broadband Photoresponse of Few-Layer Black Phosphorus Field-Effect Transistors. *Nano Lett.* **2014**, *14*, 3347−3352.

(14) Kalantar-zadeh, K.; Ou, J. Z.; Daeneke, T.; Strano, M. S.; Pumera, M.; Gras, S. L. Two-Dimensional Transition Metal Dichalcogenides in Biosystems. *Adv. Funct. Mater.* **2015**, *25*, 5086−5099.

(15) Kuc, A.; Zibouche, N.; Heine, T. Influence of Quantum Confinement on the Electronic Structure of the Transition Metal Sulfide TS_2. *Phys. Rev. B: Condens. Matter Mater. Phys.* **2011**, *83*, 245213.

(16) Kam, K. K.; Parkinson, B. A. J. Detailed Photocurrent Spectroscopy of the Semiconducting Group VIB Transition Metal Dichalcogenides. *J. Phys. Chem.* **1982**, *86*, 463.

(17) Rout, C. S.; Joshi, P. D.; Kashid, R. V.; Joag, D. S.; More, M. A.; Simbeck, A. J.; Washington, M.; Nayak, S. K.; Late, D. J. Superior Field Emission Properties of Layered WS_2-RGO Nanocomposites. *Sci. Rep.* **2013**, *3*, 3282.

(18) Katz, A.; Redlich, M.; Rapoport, L.; Wagner, H. D.; Tenne, R. Self-Lubricating Coatings Containing Fullerene-Like WS_2 Nanoparticles for Orthodontic Wires and Other Possible Medical Applications. *Tribol. Lett.* **2006**, *21*, 135−139.

(19) Georgiou, T.; Jalil, R.; Belle, B. D.; Britnell, L.; Gorbachev, R. V.; Morozov, S. V.; Kim, Y.; Gholinia, A.; Haigh, S. J.; Makarovsky, O.; Eaves, L.; Ponomarenko, L. A.; Geim, A. K.; Novoselov, K. S.; Mishchenko, A. Vertical Field-Effect Transistor Based on Graphene-WS_2 Heterostructures for Flexible and Transparent Electronics. *Nat. Nanotechnol.* **2012**, *8*, 100−103.

(20) Huo, N.; Yang, S.; Wei, Z.; Li, S.; Xia, J.; Li, J. Photoresponsive and Gas Sensing Field-Effect Transistors Based on Multilayer WS_2 Nanoflakes. *Sci. Rep.* **2014**, *4*, 5209.

(21) Navale, G. R.; Rout, C. S.; Gohil, K. N.; Dharne, M. S.; Late, D. J.; Shinde, S. S. Oxidative and Membrane Stress-Mediated Antibacterial Activity of WS_2 and rgo-WS_2 Nanosheets. *RSC Adv.* **2015**, *5*, 74726.

(22) Zong, X.; Han, J.; Ma, G.; Yan, H.; Wu, G.; Li, C. Photocatalytic H_2 Evolution on CdS Loaded with WS_2 as Co-catalyst Under Visible Light Irradiation. *J. Phys. Chem. C* **2011**, *115*, 12202−12208.

(23) Zhao, W.; Ghorannevis, Z.; Chu, L.; Toh, M.; Kloc, C.; Tan, P.; Eda, G. Evolution of Electronic Structure in Atomically Thin Sheets of WS_2 and WSe_2. *ACS Nano* **2013**, *7*, 791−797.

(24) Li, C. S.; Yan, K. H.; Fan, Z.; Shen, X. P.; Chen, K. M.; Jiang, T. S.; Hua, Y. Q.; Ding, J. N.; Yang, J. C. Synthesis and Investigation of Micro-Tribological Behavior of WS_2 Nanotube. *Mater. Sci. Forum* **2005**, *475−479*, 3521−3524.

(25) Ramakrishna Matte, H. S. S.; Gomathi, A.; Manna, A. K.; Late, D. J.; Datta, R.; Pati, S. K.; Rao, C. N. R. MoS_2 and WS_2 Analogues of Graphene. *Angew. Chem., Int. Ed.* **2010**, *49*, 4059−4062.

(26) Lauritsen, J. V.; Kibsgaard, J.; Helveg, S.; Topsøe, H.; Clausen, B. S.; Lægsgaard, E.; Besenbacher, F. Size-dependent Structure of MoS_2 Nanocrystals. *Nat. Nanotechnol.* **2007**, *2*, 53−58.

(27) Zhang, S.; Dong, N.; McEvoy, N.; O'Brien, M.; Winters, S.; Berner, N. C.; Yim, C.; Li, Y.; Zhang, X.; Chen, Z.; Zhang, L.; Duesberg, G. S.; Wang, J. Direct Observation Of Degenerate Two-Photon Absorption and its Saturation in WS_2 and MoS_2 Monolayer and Few-Layer Films. *ACS Nano* **2015**, *9*, 7142−7150.

(28) Elias, A. L.; Perea-Lopez, N.; Castro-Beltran, A.; Berkdemir, A.; Lv, R.; Feng, S.; Long, A. D.; Hayashi, T.; Kim, Y. A.; Endo, M.; Gutierrez, H. R.; et al. Controlled Synthesis and Transfer of Large-Area WS2 Sheets: From Single Layer to Few Layers. *ACS Nano* **2013**, *7*, 5235−5242.

(29) Zhao, W.; Ghorannevis, Z.; Chu, L.; Toh, M.; Kloc, C.; Tan, P. H.; Eda, G. Evolution of Electronic Structure in Atomically Thin Sheets of WS_2 and WSe_2. *ACS Nano* **2013**, *7*, 791−797.

(30) Song, J. G.; Park, J.; Lee, W.; Choi, T.; Jung, H.; Lee, C. W.; Hwang, S. H.; Myoung, J. M.; Jung, J. H.; Kim, S.-H.; et al. Layer-Controlled, Wafer-Scale, and Conformal Synthesis of Tungsten Disulfide Nanosheets Using Atomic Layer Deposition. *ACS Nano* **2013**, *7*, 11333−11340.

(31) Kalantar-zadeh, K.; Vijayaraghavan, A.; Ham, M. H.; Zheng, H.; Breedon, M.; Strano, M. S. Synthesis of Atomically Thin WO_3 Sheets from Hydrated Tungsten Trioxide. *Chem. Mater.* **2010**, *22*, 5660−5666.

(32) Perea-Lopez, N.; Elías, A. L.; Berkdemir, A.; Castro-Beltran, A.; Gutiérrez, H. R.; Feng, S.; Lv, R.; Hayashi, T.; López-Urías, F.; Ghosh, S.; Muchharla, B.; et al. Photosensor Device Based on Few-Layered WS_2 Films. *Adv. Funct. Mater.* **2013**, *23*, 5511−5517.

(33) Zhang, Y.; Zhang, Y.; Ji, Q.; Ju, J.; Yuan, H.; Shi, J.; Gao, T.; Ma, D.; Liu, M.; Chen, Y.; et al. Controlled Growth of High-Quality Monolayer WS_2 Layers on Sapphire and Imaging Its Grain Boundary. *ACS Nano* **2013**, *7*, 8963−8971.

(34) Eda, G.; Maier, S. A. Two-Dimensional Crystals: Managing Light for Optoelectronics. *ACS Nano* **2013**, *7*, 5660−5665.

(35) Buscema, M.; Island, J. O.; Groenendijk, D. J.; Blanter, S. I.; Steele, G. A.; van der Zant, H. S. J.; Castellanos-Gomez, A. Photocurrent Generation with Two-Dimensional van der Waals Semiconductors. *Chem. Soc. Rev.* **2015**, *44*, 3691−3718.

(36) Kannan, P. K.; Late, D. J.; Morgan, H.; Rout, C. S. Recent Developments in 2D Layered Inorganic Nanomaterials for Sensing. *Nanoscale* **2015**, *7*, 13293−13312.

(37) Chen, Z.; Lu, C. Humidity Sensors: a Review of Materials and Mechanisms. *Sens. Lett.* **2005**, *3*, 274−295.

(38) Wang, X.; Wang, P.; Wang, J.; Hu, W.; Zhou, X.; Guo, N.; Huang, H.; Sun, S.; Shen, H.; Lin, T.; Tang, M.; et al. Ultrasensitive and Broadband MoS_2 Photodetector Driven By Ferroelectrics. *Adv. Mater.* **2015**, *27*, 6575−6581.

DOI: 10.1021/acsami.5b11325
ACS Appl. Mater. Interfaces 2016, 8, 3359−3365

(39) Yin, Z.; Li, H.; Li, H.; Jiang, L.; Shi, Y.; Sun, Y.; Lu, G.; Zhang, Q.; Chen, X.; Zhang, H. Single-layer MoS_2 Phototransistors. *ACS Nano* **2012**, *6*, 74−80.
(40) Chen, C.; Qiao, H.; Lin, S.; Man Luk, C.; Liu, Y.; Xu, Z.; Song, J.; Xue, Y.; Li, D.; Yuan, J.; Yu, W.; et al. Highly Responsive MoS_2 Photodetectors Enhanced by Graphene Quantum Dots. *Sci. Rep.* **2015**, *5*, 11830.
(41) Qi, J.; Lan, Y. W.; Stieg, A. Z.; Chen, J. H.; Zhong, Y. L.; Li, L. J.; Chen, C. D.; Zhang, Y.; Wang, K. L. Piezoelectric Effect in Chemical Vapour Deposition-Grown Atomic-Monolayer Triangular Molybdenum Disulfide Piezotronics. *Nat. Commun.* **2015**, *6*, 7430.
(42) Yao, J. D.; Zheng, Z. Q.; Shao, J. M.; Yang, G. W. Stable, Highly-Responsive and Broadband Photodetection Based on Large-Area Multilayered WS_2 Films Grown by Pulsed-Laser Deposition. *Nanoscale* **2015**, *7*, 14974−14981.
(43) Lan, C.; Li, C.; Yin, Y.; Liu, Y. Large-Area Synthesis of Monolayer WS_2 and its Ambient-Sensitive Photo-Detecting Performance. *Nanoscale* **2015**, *7*, 5974−5980.
(44) Xia, J.; Huang, X.; Liu, L. Z.; Wang, M.; Wang, L.; Huang, B.; Zhu, D. D.; Li, J. J.; Gu, C. Z.; Meng, X. M. CVD Synthesis of Large-Area, Highly Crystalline $MoSe_2$ Atomic Layers On Diverse Substrates and Application to Photodetectors. *Nanoscale* **2014**, *6*, 8949−8955.
(45) Zhang, S.; Choi, H.; Yue, H.; Yang, W. Controlled Exfoliation of Molybdenum Disulfide for Developing Thin Film Humidity Sensor. *Current Appl. Phys.* **2014**, *14*, 264−268.
(46) Feng, J.; Peng, L.; Wu, C.; Sun, X.; Hu, S.; Lin, C.; Dai, J.; Yang, J.; Xie, Y. Giant Moisture Responsiveness of VS2 Ultrathin Nanosheets for Novel Touchless Positioning Interface. *Adv. Mater.* **2012**, *24*, 1969−1974.

DOI: 10.1021/acsami.5b11325
ACS Appl. Mater. Interfaces 2016, 8, 3359−3365

Supporting Information (SI) for

Highly Transparent Wafer Scale Synthesis of Crystalline WS_2 Nanoparticle Thin Film for Photodetector and Humidity Sensing Applications

Amit S. Pawbake[1, 2], Ravindra G. Waykar [2], Dattatray J. Late [1*] and Sandesh R. Jadkar [2*]

[1]Physical and Material Chemistry Division, CSIR – National Chemical Laboratory, Pune, 411008, Maharashtra, (India)

[2]School of Energy studies, Department of Physics, Savitribai Phule Pune University, Pune 411007, (India)

*Corresponding authors:

E-mail: dj.late@ncl.res.in / datta099@gmail.com; sandesh@physics.unipune.ac.in;

Figure S1:

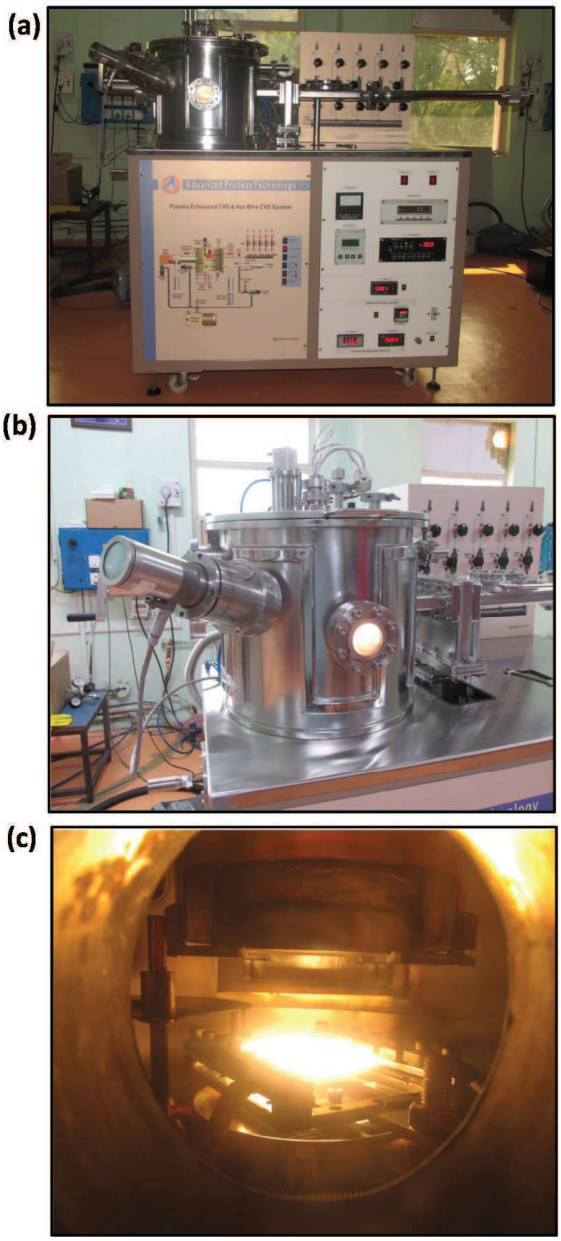

Figure S1: (a) Typical HWCVD method used for synthesized WS_2 thin film. (b) System photo taken at during deposition (c) Heated filaments at 2000^0C.

Figure S2:

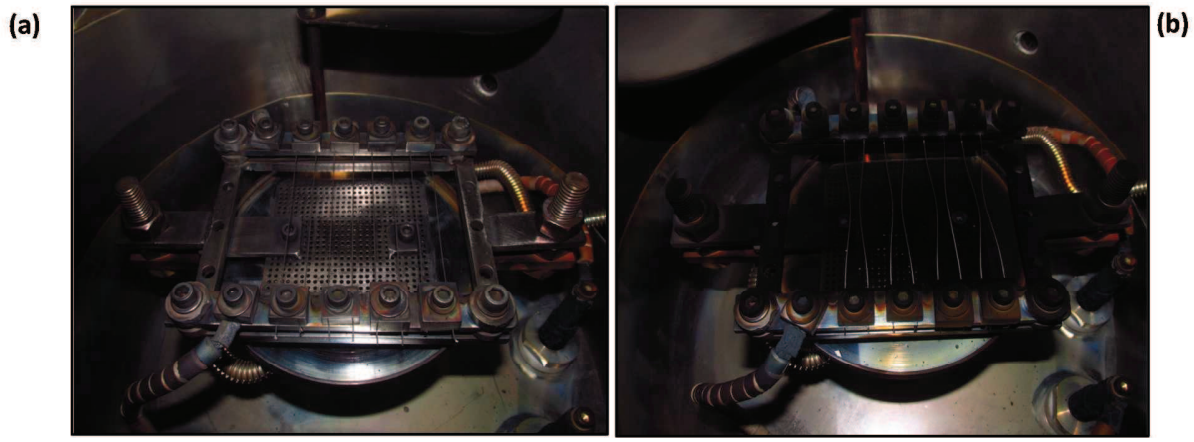

Figure S2: (a) tungsten filament arrangement (before deposition) (b) tungsten filament after deposition of WS_2 nanoparticle thin film.

Figure S3:

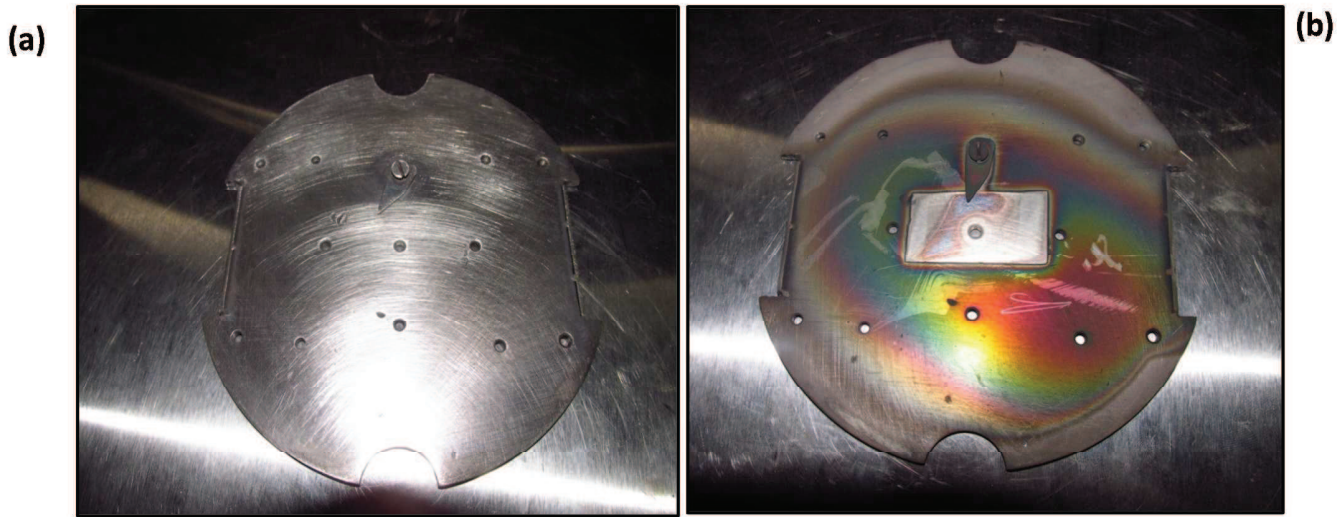

Figure S3: (a) substrate holder before deposition (b) substrate holder after deposition of WS_2 nanoparticle thin film.

Description of HW-CVD

The schematic of indigenously designed and locally fabricated dual chamber hot wire chemical vapor deposition (HW-CVD) unit used for the synthesis of WS_2 films in the present study. It consists of two stainless steel chambers, referred as process chamber and load lock chamber. The process chamber is coupled with a turbo molecular pump which yields a base pressure less than 10^{-6} Torr. Use of load lock chamber prevents the process chamber to be directly exposed to air, which minimizes the pump down time and reduce contamination of layers with oxygen and water vapors. Substrates can be moved from load lock to process chamber using pneumatically controlled transport system. The pressure during deposition was kept constant by using automated throttle valve. For deposition we have used 10 straight Tungsten (W) filaments, 1 cm apart mounted parallel to each other. Each filament has a diameter of 0.5 mm and a length of 10 cm. heating of filaments is done by an AC current using a current transformer and dimmer. The filament temperature was kept constant and measured by optical pyrometer. A shutter is placed in front of the substrates to shield the substrates from undesired deposition during pre-heating of filaments. Reaction gases were introduced in the process chamber from the bottom and perpendicular to the plane of filaments through a specially designed gas shower to ensure uniform gas flow over the filaments. The substrates can be placed on substrate holder which is heated by in build heater using K type thermocouple (chromel-alumel) and temperature controller.